Improving the chemical de-alloying of amorphous Au alloys

Improving the chemical de-alloying of amorphous Au alloys

Yanpeng Xue , Federico Scaglione, Paola Rizzi, Livio Battezzati
Dipartimento di Chimica e Centro Interdipartimentale NIS (Nanostructured Surfaces and Interfaces), Università di Torino, Via Pietro Giuria 7, 10125 Torino, Italy

Abstract

In this work, the chemical de-alloying behavior of $Au_{30}Cu_{38}Ag_7Pd_5Si_{20}$(at.%) amorphous alloy which was rapidly solidified from the melt in the form of ribbons were investigated. First a comparison between samples dealloyed in nitric acid with and without HF was conducted to achieve homogeneous de-alloying process. Then the morphology and structure of nanoporous gold (NPG) were adjusted by tuning the de-alloying parameters, such as HNO_3 concentration, electrolyte temperature and de-alloying time. Finally the surface enhanced Raman scattering(SERS) capability of the as-prepared NPG was evaluated using 4,4′-bi-pyridine as probe molecule.

1. Introduction

De-alloying is a phenomenon of corrosion where the less noble constituents of an alloy are selectively dissolved, while the noble elements diffuse along the solid/electrolyte interface into 3D interconnected open-pore structure when the alloy is contacted with an appropriate electrolyte [1]. Recently this technique is employed to prepare nanoporous metals for applications in catalysis [2,3] and electrocatalysis [4], energy storage [5], electrochemical sensors [6], and surface enhanced Raman scattering [7]. The microstructure of nanoporous metals can be controlled by adjusting the de-alloying process parameters: the amount of noble element, the electrochemical potential difference among alloy components, the critical potential for de-alloying, the composition, concentration and temperature of electrolyte. To date, many nanoporous metals and metal alloys, including gold [8,9], gold-platinum [10], silver [11,12], copper [13], have been fabricated by de-alloying method from either crystalline homogeneous solid solutions or metallic glasses precursors. Compared with crystalline alloys, a metallic glass is considered as a monolithic amorphous phase with the homogeneouschemical composition and structure [14]. During the de-alloying process, the composition range for glass formation is destroyed due to the dissolution of less noble elements and crystals must nucleate and grow to form ligaments [15,16].

Au-based metallic glasses derive from the Au-Si binary and Au-Cu-Si ternary eutectics. Schroers et al. firstly prepared a Au-Ag-Pd-Cu-Si bulk metallic glass with an Au content of about 50 at.% exhibiting high glass forming ability and high stabilization of supercooled liquid [17]. Zhang et al. developed new Au-Cu-Ag-Si metallic glass with high Au content and without the addition of Pd, which show a high glass forming ability and lower glass transition temperature [18]. These alloys are very close to or above the parting limit of Au content for de-alloying to prepare nanoporous materials. More recently, Guo et al. prepared Au-Ag-Pd-CuSi metallic glassy alloys with low Au contents by substitution Au with Cu, in which $Au_{40}Cu_{28}Ag_7Pd_5Si_{20}$(at.%) shows the best glass forming ability [19]. Nanoporous gold can be prepared from this metallic glass precursor by chemical or electrochemical de-alloying in the form of ribbon [20,21]. Normally, during the rapid solidification process of this alloy, a native SiO_2 layer is formed on the ribbon surface [22], and in the early stage of de-alloying isolated nanocrystals germinate when the electrolyte penetrates through the cracks of this layer [16]. However, when this Au-based amorphous alloys were de-alloyed chemically in nitric acid solution, silica patches were always present randomly on nanoporous gold ligaments, which influences their potential applications [20].

In this paper, the addition of HF in HNO_3 was used to solve this problem and investigate the chemical de-alloying behavior of $Au_{30}Cu_{38}Ag_7Pd_5Si_{20}$(at.%) metallic glass precursor in various conditions. In a previous work, nanoporous gold was fabricated by electrochemical de-alloying from this metallic glass precursor with ligament size between 75 and 200 nm [23], which was used as SERS substrate reaching a sensitivity up to 10^{-11} M using 4,4′-bi-pyridine as probe molecules. In this work the SERS capability of the as-prepared NPG by chemical de-alloying was also examined using the same probe molecule.

2. Experimental

A $Au_{30}Cu_{38}Ag_7Pd_5Si_{20}$(at.%) master alloy was prepared by arc melting the pure elements (Au: 99.99%, Ag, Cu, Pd: 99.99%, Si: 99.9995%) in Ti-gettered Argon atmosphere. The ingot was rapidly

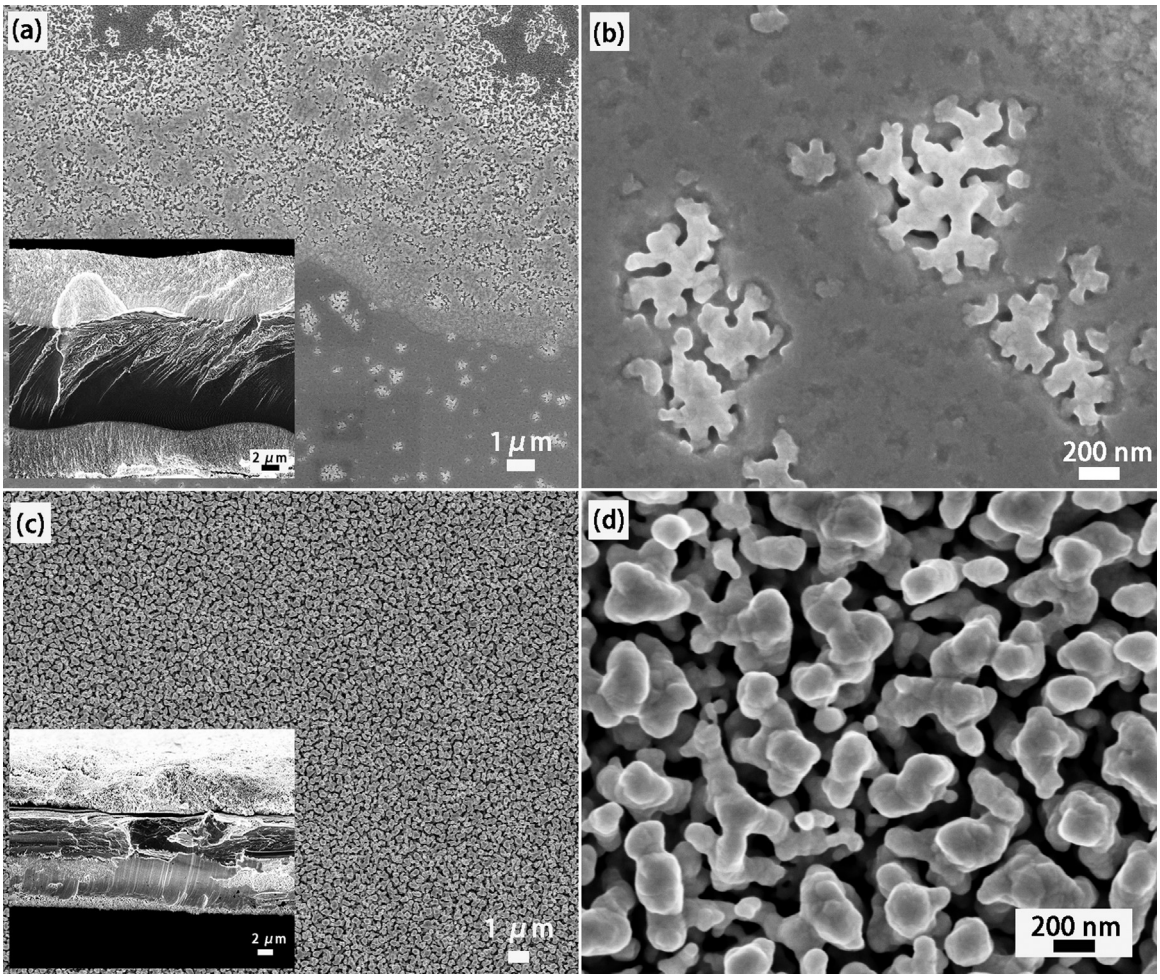

Fig 1. SEM images after chemically de-alloyed for 26 days at room temperature:(a) and (b) in 10 M HNO_3.(c) and (d) in 10 M HNO_3 + 0.5 M HF. (b) and (d) are the enlargement of (a) and (c) respectively.The insets show the corresponding cross section of de-alloyed samples.

solidified onto a rotating copper wheel in a closed chamber kept under Ar protective atmosphere at a linear speed of 25 m/s by the meltspinning process. The thickness of the resulting amorphous ribbon is around 25 μm and the width is around 2 mm. Samples around 20 mm in length were cut for chemical de-alloying.

Chemical de-alloying of the as-spun ribbons was conducted in solution of HNO_3 with and without 0.5 M HF at various conditions. To study the effect of HF on the surface morphology, the samples were chemically de-alloyed for 26 days at room temperature in 10 M HNO_3 with and without 0.5 M HF.To investigate the effect of electrolyte temperature, chemical de-alloying was performed as a function of temperature in 10 M HNO_3 and 0.5 M HF solution for 6 h. To find the effect of HNO_3 concentration on the characteristic length scale, different concentrations of 3, 5, 10 and 14.4 M HNO_3 were used and different de-alloying times of 30 min, 1, 2, 4 and 6 h were applied to study the microstructure evolution. After chemical de-alloying, the as-prepared samples were deeply rinsed with distilled water and then dried for investigation.

The surface morphology of de-alloyed samples was observed by Scanning Electron Microscopy (SEM) and their compositions were checked by Energy Dispersive X-ray Spectroscopy (EDS) after Co calibration. A Panalytical X′Pert X-Ray equipment was used to study the microstructure of the de-alloyed materials with monochromatic Cu Kα (λ = 1.5418A°) radiation in Bragg-Brentano mode.

Micro-Raman measurements were performed with a Renishaw inVia Raman Microscope using 785 nm laser line with an acquisition time of 20 s, 0.02 mW power at the sample and a 50 × ULWD objective; 4,4′bipyridine (bipy) was chosen as SERS probe molecules. Prior to SERS experiments, the nanoporous gold samples were cleaned in concentrated nitric acid for 5 min and rinsed several times in de-ionized water. Then, the de-alloyed samples were immersed in ethanol solution of 4,4′-bipyridine with concentration from 10^{-14} M to 10^{-11} M for one night, enabling the probe molecules to be adsorbed on the surface. Measurements were performed on the surface of sample after drying in air. SERS intensity mapping image of 48 × 48 μm^2 area with a step length of 4 μm was collected using bipyridine concentration of 10^{-13} M through monitoring the characteristic peak at 1619 cm^{-1}. All solutions were prepared from chemical grade reagents and de-ionized water. The Raman band of silicon wafer at 520 cm^{-1} was used to calibrate the spectrometer.

3. Results and discussion

3.1. Effect of HF on the surface morphology

To illustrate the effect of HF on the morphology of de-alloyed samples, a comparison between de-alloying in nitric acid with and without HF was performed. Fig. 1 shows the SEM images after chemical de-alloying for 26 days at room temperature in 10 M HNO_3 with and without 0.5 M HF. Without the addition of HF in solution, the de-alloying process occurs inhomogeneously on the whole surface. Some parts were de-alloyed, and other parts were passivated(Fig. 1a). From the cross section of de-alloyed part, it is deduced that the de-alloyed thickness is not identical even in this part, which indicates the de-

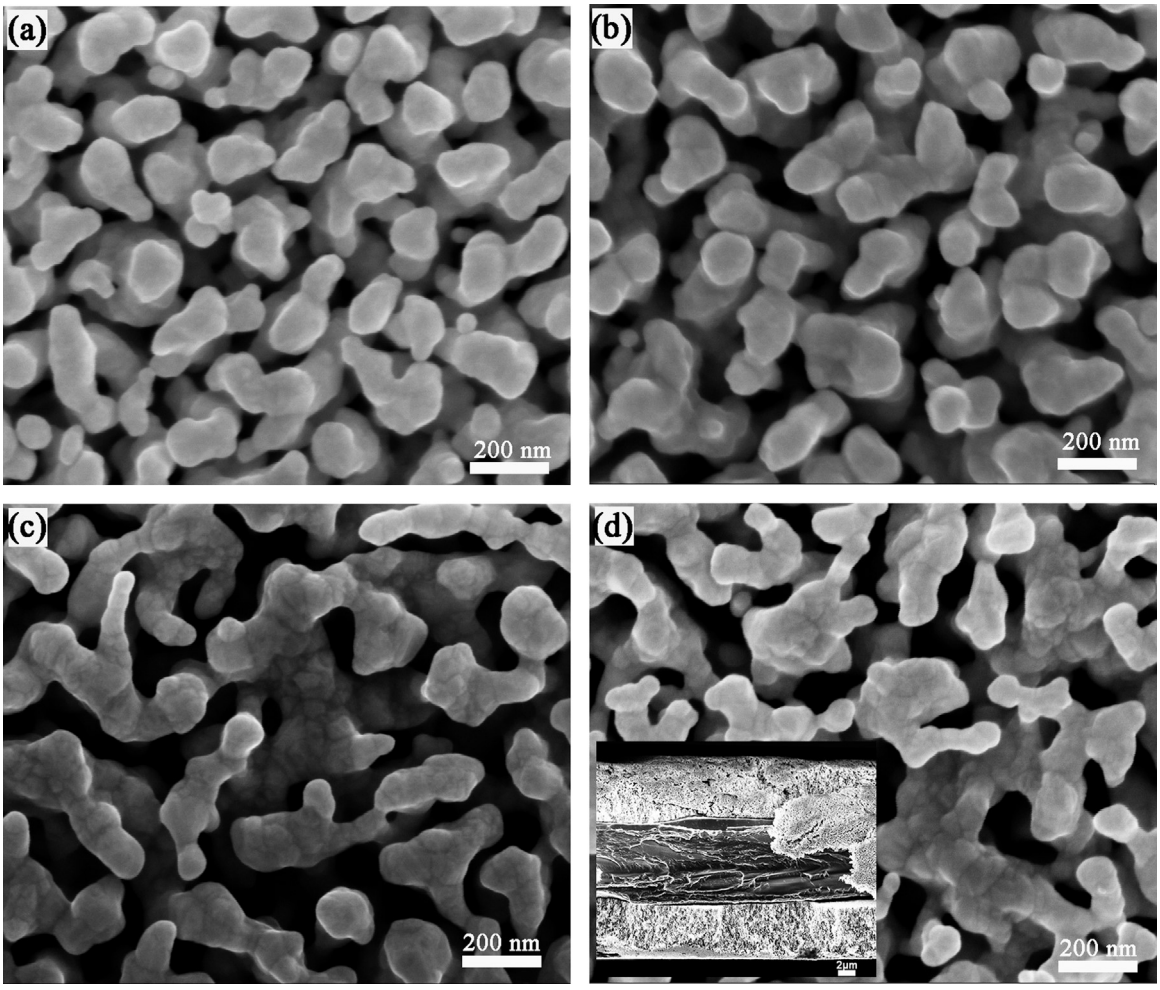

Fig. 2. SEM images after chemically de-alloyed in 10 M HNO_3 + 0.5 M HF for 6 h at temperatures: (a) 40 °C, (b) 50 °C, (c) 70 °C, (d) 80 °C. The inset shows the corresponding cross section of de-alloyed sample.

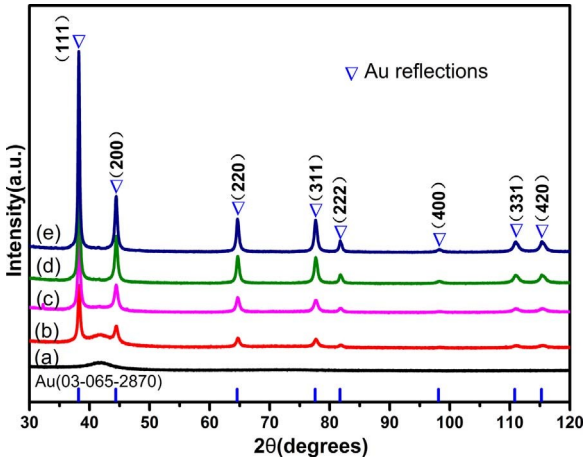

Fig. 3. XRD patterns of (a) the as-spun $Au_{30}Cu_{38}Ag_7Pd_5Si_{20}$(at.%) ribbon and samples chemically de-alloyed in 10 M HNO_3 + 0.5 M HF for 6 h at different temperatures:(b) 40 °C, (c) 50 °C, (d) 70 °C and (e) 80 °C.

alloyed process occurs inhomogeneously. In the passivated parts, many small de-alloyed zones can be observed and small ligaments of nanoporous gold were formed(Fig. 1b). This indicates that local chemical inhomogeneity exists on the surface of the as-spun ribbon, especially the inhomogeneous distribution of silicon. In fact, performing the same experiment in the mixed solution of 10 M HNO_3 and 0.5 M HF, the ligaments of nanoporous gold were obtained on the whole surface (Fig. 1c).The cross section of ribbon indicates that the de-alloying process occurs uniformly. The ligament size is around 150 nm and there are many small ligaments in between large ones(Fig. 1d). This results clearly demonstrates that the homogeneous de-alloying process can be achieved by the addition of HF in nitric solution when local chemical inhomogeneity occurs on the surface of the as-spun ribbon.

3.2. Effect of the electrolyte temperature and de-alloying time on surface morphology

Since the de-alloying process includes the dissolution of less-noble elements and the self-organization of noble elements by surface diffusion, electrolyte temperature is apparently an important parameter to tailor the resultant nanoporous microstructure. Fig. 2a–d show the surface morphologies of the de-alloyed samples prepared in 10 M HNO_3 + 0.5 M HF solution at 40 °C, 50 °C, 70 °C and 80 °C, respectively. It is seen that at low de-alloying temperature, the ligaments grow separately, and the distribution of ligaments is more homogeneous. However at high de-alloying temperature, the ligaments coalesce into larger blocks. By increasing the electrolyte temperature from 40 °C to 80 °C, the ligament size increases from ~ 100 nm to ~155 nm (Fig.S1).As shown in Fig.S1, the thickness of the de-alloyed layer increases from 1.7 μm to 13.7 μm when the electrolyte temperature increases from 40 °C to 80 °C, implying that the dissolution rate of less noble element and surface diffusion rate of noble element increase with electrolyte temperature.

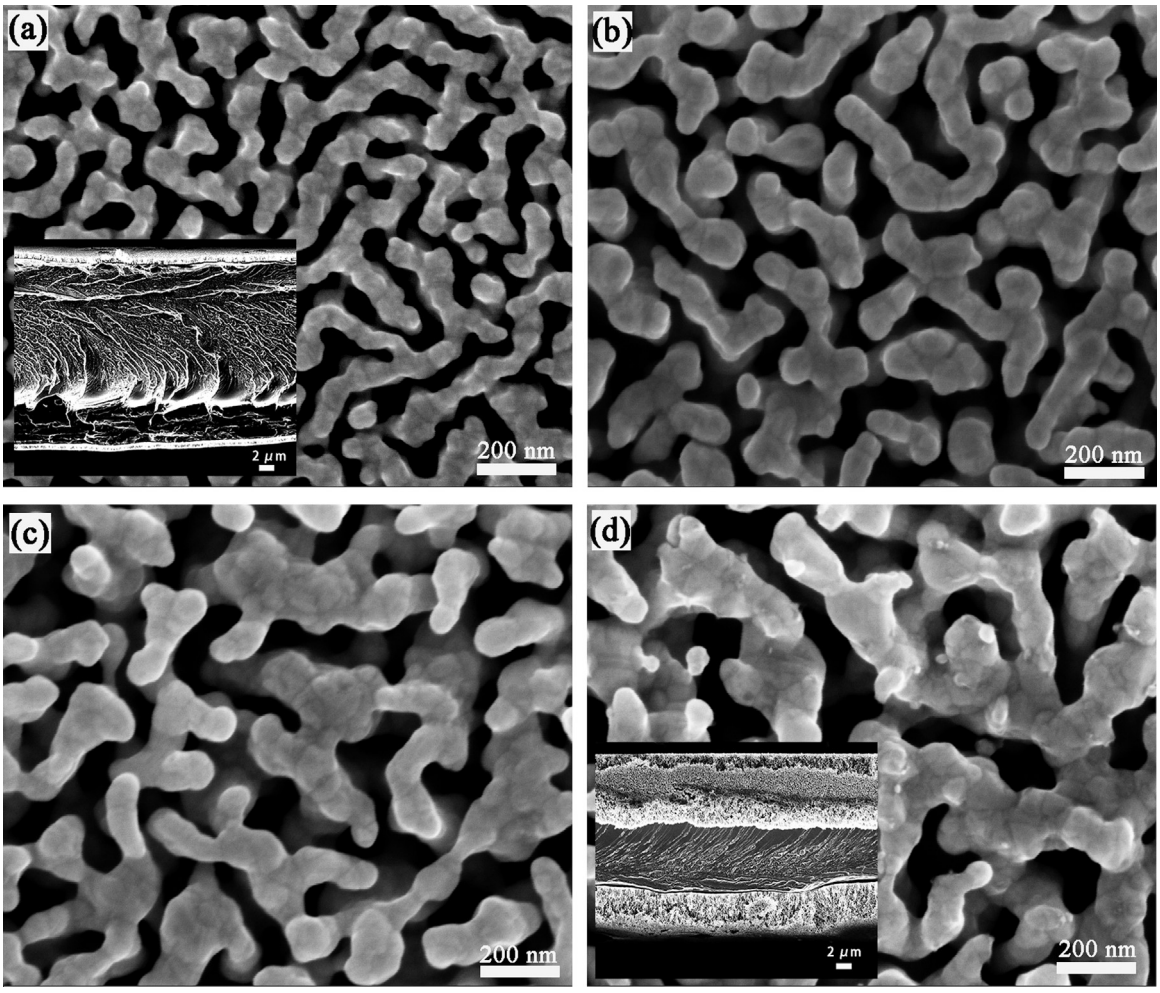

Fig. 4. SEM images after chemically de-alloying at 70 °C for 6 h under HNO_3 concentration:(a) 3 M HNO_3+ 0.5 M HF; (b) 5 M HNO_3 + 0.5 M HF; (c) 10 M HNO_3 + 0.5 M HF; (d) 14.4 M HNO_3 + 0.5 M HF. The inset shows the corresponding cross section of de-alloyed sample.

The XRD patterns of de-alloyed samples in the mixture of 10 M HNO_3 and 0.5 M HF for 6 h at different electrolyte temperatures are shown in Fig. 3. At low electrolyte temperature of 40 °C, the amorphous broad halo representative of glassy state is still visible after chemical de-alloying for 6 h, which is in agreement with the limited thickness of de-alloyed samples(Fig.S1).With the increase of electrolyte temperature, the thickness of de-alloyed layer increases and the peak intensity of fcc Au become stronger. According to the Rietveld method, the size of scattering domains was evaluated and given in Table S1 showing a temperature dependence. The size of ligaments made of several domain increases accordingly.

The microstructure evolution of $Au_{30}Cu_{38}Ag_7Pd_5Si_{20}$ ribbons was also studied at different de-alloying times from 30 min to 6 h in 10 M HNO_3 + 0.5 M HF at 70 °C(Fig.S2). After chemical de-alloying for 30 min, the Au ligaments start to form separately with size of 75 nm. On continuation of the process, both thickness of the de-alloyed layer and ligament size increase. When the de-alloying time increases to 2 h, short ligaments connect to form long ligaments. With further increase of dealloying time, ligaments coalesce with neighbors to form larger ligaments. In all case the growth is due to Au surface diffusion. Accompanied with the dissolution of less noble elements, the size of ligament increases from 70 to 125 nm with de-alloying time, and the thickness of the de-alloyed layer increases steadily via the movement of the de-alloying front. EDS quantitative analysis confirmed that the content of Au increases and the amount of less noble elements decreases gradually with the increase of de-alloying time(Fig.S3). And the XRD patterns clearly demonstrate the structure evolution from the glassy state to the fcc Au with the increase of de-alloying time(Fig.S4).

3.3. Effect of the HNO_3 concentration on surface morphology

Fig. 4a–d show the typical morphology of the de-alloyed Au based metallic glass in the mixed solutions of 0.5 M HF and HNO_3 concentration of 3 M, 5 M, 10 M and 14.4 M for 6 h, respectively. When the concentration of HNO_3 is 3 M, the ligaments size is around 60 nm after de-alloying for 6 h. The distribution of ligaments and pores is homogeneous. From the cross section of de-alloyed sample, the de-alloyed layer is limited (Fig. 4a). With the increase of HNO_3 concentration to 5 M, and to 10 M, ligaments grow and merge with neighboring ones. Large ligaments are formed at 14.4 M HNO_3. The thickness of de-alloyed layer increases to 14.7 μm after de-alloying for 6 h (Fig. 4d).From the plot of ligament size versus HNO_3 concentration (Fig.S5), the ligament size increases to ⍰150 nm (Fig. 4d)when the HNO_3 concentration in the mixture increases to 14.4 M.

3.4. SERS effect of nanoporous gold

In order to demonstrate the SERS capability, samples de-alloyed in different HNO_3 concentrations were examined first. Fig. 5a shows the SERS spectra of samples chemically de-alloyed at 70 °C for 6 h in different HNO_3 concentrations after immersing them for one night in ethanol solution of 10^{-11} M bipyridine. When the sample de-alloyed in the mixed solution with 3 M HNO_3 is used as Raman substrate, no characteristic peak of bipyridine is observed. With the increase of HNO_3

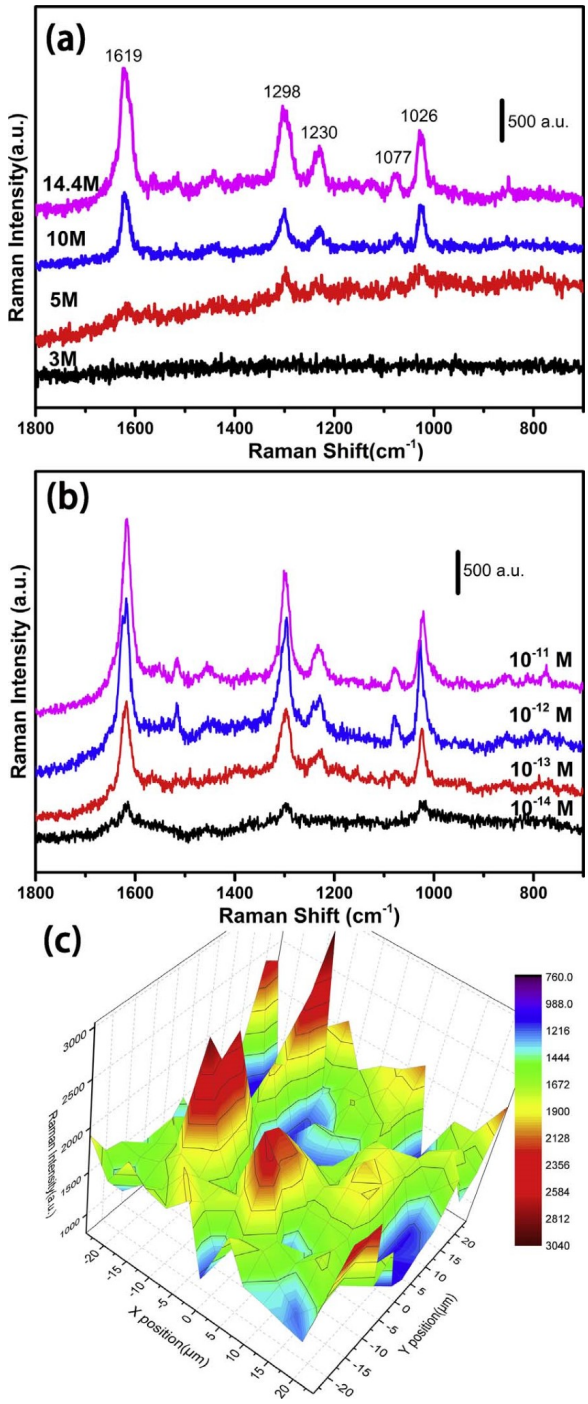

Fig. 5. (a) SERS spectra of 10^{-11} M 4,4′-bipyridine on samples de-alloyed at 70 °C for 6 h in mixture solution with increasing HNO_3 concentration. (b)SERS spectra of 4,4′-bipyridine at different concentrations on de-alloyed samples. (c) SERS intensity mapping image of 48 × 48 μm^2 with bipyridine concentration of 10^{-13} M based on characteristic peak at 1619 cm^{-1}. The laser wavelength was 785 nm with an acquisition time of 20 s for a single measurement.

concentration to 5 M, the Raman characteristic peaks of bipyridine at 1616, 1297, and 1026 cm^{-1} become visible [24,25]. And the SERS intensity of main characteristic peaks increase by using the substrate de-alloyed in higher HNO_3 concentration. Although the ligament size of nanoporous gold increase with the HNO_3 concentration, the SERS inactive elements become less under the same de-alloying conditions. Therefore the sample de-alloyed in 14.4 M HNO_3 shows the strongest Raman response which is consistent with our recent findings [23].

The Raman spectra shown in Fig. 5(b) are the most intense ones with bipyridine concentrations varying from 10^{-14} M to 10^{-11}M on the sample de-alloyed in 14.4 M HNO_3 plus 0.5 M HF at 70 °C for 6 h. The Raman intensity of characteristic peaks decreases as bipyridine concentration decreased. For the solution with concentration of 10^{-14} M, the three characteristic peaks at 1616, 1297, and 1026 cm^{-1} were distinguishable. This result demonstrates that the detection limit for bipyridine adsorbed on the surface of this NPG substrate is as low as 10^{-14} M. This result is better than our previous work where the SERS active substrate was prepared by electrochemical de-alloying from this Au based metallic glass precursor [23]. Fig. 5(c) shows a SERS intensity mapping image based on the characteristic peak at 1619 cm^{-1}, which clearly demonstrates the presence of "hot spots". Strong spot-to-spot variation can be observed which is associated with the adsorption status of each molecule and the localized electromagnetic field variation at each spot [26]. Recently, Zhang et al. demonstrate the single molecule SERS detection using sharp gold nanocones substrate which is prepared by plating gold on nanoporous gold de-alloyed from crystalline alloys utilizing the open nanopore channels of nanoporous gold as template [26]. The high SERS effect is attributed to the localized electromagnetic field enhancement around the sharp apexes of nanocones on nanoporous gold film. In our case, the high enhancement of SERS effect comes from the localized surface plasmons within the main microstructural features of three dimensional nanoporous gold such as interconnected ligaments, surface grooves and defects [27]. Therefore the SERS enhancement of our samples can be attributed to the local electromagnetic field enhancement around nanopores and the electromagnetic coupling effect between adjacent gold ligaments [28,29]. Moreover, in comparison with the nanoporous gold de-alloyed from the crystalline alloy which retains the original grains, the ligaments are constituted by several nanocrystals with random orientation and separated by grain boundaries when the nanoporous gold is prepared from amorphous alloy, which may generate more "hot spots", leading to the further enhancement of SERS effect [30].

4. Conclusions

In summary, we reported the chemical de-alloying behavior of a Au based metallic glass. The addition of HF in HNO_3 solution was used to eliminate silica patches for achieving homogeneous de-alloying. By tuning the de-alloying parameters, such as HNO_3 concentration and electrolyte temperature, the gold ligaments can be adjusted ranging from 60 to 150 nm in the mixed solution of HNO_3 and HF. The SERS capability on samples de-alloyed in different HNO_3 concentrations was compared: the sample de-alloyed in the highest HNO_3 concentration shows best Raman response. On this best SERS active substrate a detection limit down to 10^{-14} M can be achieved. The enhancement of SERS effect on nanoporous gold is attributed to the localized enhanced electromagnetic fields around nanopores, the electromagnetic coupling between ligaments. Ligaments constituted by several nanocrystals with random orientation and separated by grain boundaries leads to further enhancement of SERS effect.

Acknowledgements

Dr Alessandro Damin of Centro Interdipartimentale NIS (Nanostructured Surfaces and Interfaces), Università di Torino, is kindly acknowledged for the SERS experiments. This work was supported by the funding scheme of the European Commission, Marie Curie Actions-Initial Training Networks (ITN) in the frame of the project VitriMetTech-Vitrified Metals Technologies and Applications in Devices and Chemistry, 607080 FP7-PEOPLE-2013-ITN, and also by BINGO Project–Torino call2014 L2 146 and Compagnia di SanPaolo.

References

[1] I. Mccue, E. Benn, B. Gaskey, J. Erlebacher, Dealloying and dealloyed materials, Annu. Rev. Mater Res. 46 (2015) 1–24, http://dx.doi.org/10.1146/annurev-matsci-070115-031739.

[2] A. Wittstock, V. Zielasek, J. Biener, C.M. Friend, M. Bäumer, Nanoporous gold catalysts for selective methanol at low temperature, Science 327 (2010) 319–322, http://dx.doi.org/10.1126/science.1183591.

[3] J. Biener, M.M. Biener, R.J. Madix, C.M. Friend, Nanoporous gold understanding the origin of the reactivity of a 21 st century catalyst made by pre-Columbian technology, ACS Catal. 5 (2015) 6263–6270, http://dx.doi.org/10.1021/acscatal. [20] 5b01586.

[4] Q. Lu, G.S. Hutchings, W. Yu, Y. Zhou, R.V. Forest, R. Tao, J. Rosen, B.T. Yonemoto, Z. Cao, H. Zheng, J.Q. Xiao, F. Jiao, J.G. Chen, Highly porous non-precious bime-metallic electrocatalysts for efficient hydrogen evolution, Nat. Commun. 6 (2015) 6567, http://dx.doi.org/10.1038/ncomms7567.

[5] R. Li, X. Liu, H. Wang, Y. Wu, Z.P. Lu, Development of electrochemical super-capacitors with uniform nanoporous silver network, Electrochim. Acta. 182 (2015) 224–229, http://dx.doi.org/10.1016/j.electacta.2015.09.069.

[6] X.-Y. Lang, H.-Y. Fu, C. Hou, G.-F. Han, P. Yang, Y.-B. Liu, Q. Jiang, Nanoporous gold supported cobalt oxide microelectrodes as high-performance electrochemical biosensors, Nat. Commun. 4 (2013) 2169, http://dx.doi.org/10.1038/ ncomms3169.

[7] L. Zhang, X. Lang, A. Hirata, M. Chen, Wrinkled nanoporous gold films with ultrahigh surface-enhanced raman scattering enhancement, ACS Nano. 5 (2011) 4407–4413, http://dx.doi.org/10.1021/nn201443p.

[8] Y. Ding, Y.J. Kim, J. Erlebacher, Nanoporous gold leaf: ancient technology/advanced material, Adv. Mater. 16 (2004) 1897–1900, http://dx.doi.org/10.1002/ adma.200400792.

[9] L.H. Qian, M.W. Chen, Ultrafine nanoporous gold by low-temperature dealloying and kinetics of nanopore formation, Appl. Phys. Lett. 91 (2007) 083105, http://dx.doi.org/10.1063/1.2773757.

[10] A.A. Vega, R.C. Newman, Nanoporous metals fabricated through electrochemical dealloying of Ag-Au-Pt with systematic variation of Au:Pt ratio, J. Electrochem. Soc. 161 (2013) C1–C10, http://dx.doi.org/10.1149/2.003401jes. [27]

[11] L. Zhang, L. Chen, H. Liu, Y. Hou, A. Hirata, T. Fujita, M. Chen, Effect of residual silver on surface-enhanced raman scattering of dealloyed nanoporous gold, J. Phys. Chem. C. 115 (2011) 19583–19587, http://dx.doi.org/10.1021/jp205892n. [28]

[12] M. Zhang, A.M. jorge junior, S.J., pang, T., zhang, A.R. yavari, fabrication of nanoporous silver with open pores, Scr. Mater. 100 (2015) 21–23, http://dx.doi.org/ 10.1016/j.scriptamat.2014.11.040.

[13] R. Li, X. Liu, H. Wang, Y. Wu, Z.P. Lu, Bendable nanoporous copper thin films with tunable thickness and pore features, Corros. Sci. 104 (2016) 227–235, http://dx. doi.org/10.1016/j.corsci.2015.12.015.

[14] J. Yu, Y. Ding, C. Xu, A. Inoue, T. Sakurai, M. Chen, Nanoporous metals by dealloying multicomponent metallic glasses, Chem. Mater. 20 (2008) 4548–4550, http://dx.doi.org/10.1021/cm8009644.

[15] P. Rizzi, F. Scaglione, L. Battezzati, Nanoporous gold by dealloying of an amorphous precursor, J. Alloys Compd. 586 (2014) S117–S120, http://dx.doi.org/10.1016/j. jallcom.2012.11.029.

[16] E.M. Paschalidou, F. Celegato, F. Scaglione, P. Rizzi, L. Battezzati, A. Gebert, S. Oswald, U. Wolff, L. Mihaylov, T. Spassov, The mechanism of generating nanoporous Au by de-alloying amorphous alloys, Acta Mater. 119 (2016) 177–183, http://dx.doi.org/10.1016/j.actamat.2016.08.025.

[17] J. Schroers, B. Lohwongwatana, W.L. Johnson, A. Peker, Gold based bulk metallic glass, Appl. Phys. Lett. 87 (2005) 061912, http://dx.doi.org/10.1063/1.2008374.

W. Zhang, H. Guo, M.W. Chen, Y. Saotome, C.L. Qin, A. Inoue, New Au-based bulk glassy alloys with ultralow glass transition temperature, Scr. Mater. 61 (2009) 744–747, http://dx.doi.org/10.1016/j.scriptamat.2009.06.020.

[18] H. Guo, W. Zhang, C. Qin, J. Qiang, M. Chen, A. Inoue, Glass-Forming ability and properties of new au-Based glassy alloys with low Au concentrations, Mater. Trans. 50 (2009) 1290–1293, http://dx.doi.org/10.2320/matertrans.ME200809.

F. Scaglione, P. Rizzi, F. Celegato, L. Battezzati, Synthesis of nanoporous gold by free corrosion of an amorphous precursor, J. Alloys Compd. 615 (2014) S142–S147, http://dx.doi.org/10.1016/j.jallcom.2014.01.239.

F. Scaglione, P. Rizzi, L. Battezzati, De-alloying kinetics of an Au-based amorphous alloys, J. Alloys Compd. 536S (2012) S60–S64, http://dx.doi.org/10.1016/j. jallcom.2011.11.087.

S. Kaciulis, A. Mezzi, G. Fiore, I. Ichim, L. Battezzati, P. Rizzi, XPS study of goldbased metallic glass, Surf. Interface Anal. 42 (2010) 597–600, http://dx.doi.org/10. 1002/sia.3231.

F. Scaglione, E.M. Paschalidou, P. Rizzi, S. Bordiga, L. Battezzati, E.M. Paschalidou, P. Rizzi, S. Bordiga, L. Battezzati, Nanoporous gold obtained from a metallic glass precursor used as substrate for surface-enhanced Raman scattering, Philos. Mag. Lett. 95 (2015) 474–482, http://dx.doi.org/10.1080/09500839.2015.1093665. S.W. Joo, Surface-enhanced Raman scattering of 4,4′-bipyridine on gold nanoparticle surfaces, Vib. Spectrosc. 34 (2004) 269–272, http://dx.doi.org/10.1016/j. vibspec.2003.12.006.

M. Suzuki, Y. Niidome, S. Yamada, Adsorption characteristics of 4,4'-bipyridine molecules on gold nanosphere films studied by surface-enhanced Raman scattering, Thin Solid Films 496 (2006) 740–747, http://dx.doi.org/10.1016/j.tsf.2005.09. 114.

L. Zhang, H. Liu, L. Chen, P. Guan, B. Chen, T. Fujita, Y. Yamaguchi, H. Iwasaki, Q.-K. Xue, M. Chen, Large-scale growth of sharp gold nano-cones for single-molecule SERS detection, RSC Adv. 6 (2016) 2882–2887, http://dx.doi.org/10.1039/ C5RA22321K.

K.L. Kelly, E. Coronado, L.L. Zhao, G.C. Schatz, The optical properties of metal nanoparticles the influence of size shape, and dielectric environment, J. Phys. Chem. B. 107 (2003) 668–677.

L.H. Qian, X.Q. Yan, T. Fujita, A. Inoue, M.W. Chen, Surface enhanced Raman scattering of nanoporous gold: smaller pore sizes stronger enhancements, Appl. Phys. Lett. 90 (2007) 153120, http://dx.doi.org/10.1063/1.2722199.

X. Lang, P. Guan, L. Zhang, T. Fujita, M. Chen, Characteristic length and temperature dependence of surface enhanced Raman scattering of nanoporous gold, J. Phys. Chem. C. 113 (2009) 10956–10961, http://dx.doi.org/10.1021/jp903137n.

R. Li, X.J. Liu, H. Wang, Y. Wu, X.M. Chu, Z.P. Lu, Nanoporous silver with tunable pore characteristics and superior surface enhanced Raman scattering, Corros. Sci. 84 (2014) 159–164, http://dx.doi.org/10.1016/j.corsci.2014.03.023.